

Research Article

Comparing the Capability of Phenomenological (Johnson-Cook and Arrhenius-Type) and Artificial Neural Network Models in Predicting the Hot Deformation Behavior of Additively Manufactured 316L Stainless Steel

A. Esmailpour and H.R. Abedi*

School of Metallurgy & Materials Engineering, Iran University of Science and Technology (IUST), Tehran, Iran

ARTICLE INFO

Article history:

Received 21 June 2022
 Reviewed 17 July 2022
 Revised 24 July 2022
 Accepted 24 July 2022

Keywords:

Additive manufacturing
 Stainless steel
 Hot deformation behavior
 Arrhenius-type model
 Artificial neural network

ABSTRACT

The high temperature flow behavior of additively manufactured 316L stainless steel was investigated in this study by hot compression tests at the temperatures of 973, 1073, 1173 and 1273 K and strain rates of 0.001-0.1 s⁻¹. Constitutive models consisting of Johnson-Cook and Arrhenius-type were employed. The results indicated that the Arrhenius-type constitutive equation had higher accuracy than the Johnson-Cook model, but these constitutive models could not predict (i) the strength levels at all temperatures and strain rates, and (ii) the flow hardening/softening behavior, accurately. Therefore, an artificial neural network with a feed-forward back propagation learning algorithm has been established to predict the high temperature flow behavior of additively manufactured 316L stainless steel. This model includes three layers namely the input layer, the hidden layer (with 20 neurons), and the output layer. The input data consisted of true strain (ϵ), strain rate ($\dot{\epsilon}$), and deformation temperature (T) while the predicted flow stress (σ) was the output data. In order to evaluate the performance of employed models, standard statistical parameters such as the average absolute relative error (AARE), root mean square error (RMSE) and correlation coefficients (R) were used. The results showed that the artificial neural network model was more accurate than the constitutive equations in predicting the high temperature flow behavior of additively manufactured 316L stainless steel.

© Shiraz University, Shiraz, Iran, 2022

1. Introduction

Additive manufacturing (AM) capable of building parts from 3D computer-aided-design (CAD) data [1, 2] has been developed significantly in the past two decades. In this method, a wide range of materials including polymers, ceramics and metals can be produced [3]. Additive manufacturing is popular due to its particular properties, such as production of complex geometry

components, lower material wastage and reduction or elimination of post-processes [4]. One of the most important powder bed additive manufacturing technologies is selective laser melting (SLM) which uses a focused laser beam to bind powders together in a layer under a protective atmosphere and this process is repeated for each layer until the final part is completed [5-7]. The high cooling rates (10³-10⁸ K/s) of SLM leads to fine microstructure which enhances strength and

* Corresponding author
 E-mail address: habedi@iust.ac.ir (H.R. Abedi)
<https://doi.org/10.22099/IJMF.2022.43705.1231>

ductility [8, 9]. The 316L stainless steel is a popular alloy that has been widely used in several applications such as marine, biomedical and the petrochemical industry [10, 11] due to its mechanical properties and excellent corrosion resistance [2].

Mathematical simulation and modeling of high temperature flow stress are very important in optimizing the hot working processes [12, 13]. Various constitutive equations, consisting of phenomenological and physical-based models, have been developed to predict the flow behavior of different materials [14]. The capability of constitutive models has been investigated for different types of steels by many researchers [15-18]. The Johnson-Cook model [19] is one of the famous phenomenological constitutive models, the capability of which has been assessed in the case of magnesium alloys [20, 21], aluminum alloys [22, 23], various grades of steels [24-28] and titanium alloys [29, 30]. The Johnson-Cook model expresses the dependence of flow stress on imposed strain, strain rate and deformation temperature [14]. Another phenomenological constitutive model is hyperbolic sine Arrhenius-type [31] which has been successfully utilized in predicting the hot flow behavior of materials [32]. Abbasi-Bani et al. [20] applied the Johnson-Cook and Arrhenius-type models for flow stress prediction of the Mg-6Al-Zn alloy, the results of which showed that Arrhenius-type equation is more accurate than Johnson-Cook model.

The parameters affecting flow stress have a non-linear relationship. Therefore, an accurate model is needed to predict the flow behavior of materials during hot deformation [33]. Artificial neural network (ANN) is an artificial intelligence method that is appropriate to extract non-linear and complex relationships. ANN learns from training data and recognizes patterns without any physical knowledge about deformation parameters. The main advantage of the ANN model is that there is

no need to postulate any mathematical models [34-37]. ANN has been successfully utilized in accurately predicting hot deformation behavior of materials [38-40]. Yang et al. [41] used a feed-forward back propagation ANN model to predict the high temperature flow behavior of 7075 Aluminum alloy. Rezaei-Ashtiani et al. [32] predicted the hot deformation behavior of Al-Cu-Mg-Pb alloy through the Johnson-Cook, Arrhenius-type and ANN models, and the results indicated that the ANN model is more accurate than the phenomenological constitutive models.

The present study has compared the capability of phenomenological constitutive models (Johnson-Cook and Arrhenius-type) and an artificial neural network model with a back propagation learning algorithm to predict the hot flow behavior of SLMed 316L stainless steel. The predictability of these models was evaluated by using standard statistical parameters. The outcomes are expected to increase knowledge regarding the post-processing routes and servicing capability of additively manufactured steels.

2. Experimental Procedure

In this study, the NOURA M100 SLM machine was employed to fabricate the specimens. The SLM process parameters such as scanning speed, maximum laser power, hatch spacing and layer thickness are shown in Table 1. The process was carried out under the protective atmosphere of argon gas. The manufactured specimens were formed in a 8 mm by 12 mm cylindrical shape (according to the ASTM-E209 standard [42]). Gas-atomized 316L stainless steel powders with spherical morphology and average diameter of 45 μm were utilized as the starting material of SLM process. The chemical composition of 316L stainless steel powder is given in Table 2.

Table 1. The SLM process parameters

Scanning speed(mm/s)	Maximum laser power(w)	Hatch spacing(μm)	Layer thickness(μm)	No. of Layer
750	300	75	30	402

Table 2. The chemical composition of gas-atomized 316L powders

Element	Cr	Ni	Mo	Mn	Si	C	P	Fe
wt.%	17.13	11.1	2.4	1.4	0.45	0.03	0.029	Balance

The hot compression tests were conducted at the temperatures of 973-1273 K under the strain rates of 0.001, 0.01 and 0.1 s⁻¹. The cylindrical specimens were preheated at deformation temperatures and were held for 5 min to eliminate the temperature gradient. Thin mica sheets were utilized to reduce the friction effects. The specimens deformed up to the true strain of 0.6 and after deformation, they were immediately quenched into water.

3. Results and Discussion

3.1. High temperature flow stress curves

The true stress-true strain curves of SLMed 316L stainless steel gained from the hot compression tests at the temperatures of 973-1273 K and strain rates of 0.001, 0.01 and 0.1 s⁻¹ are shown in Fig. 1. It can be seen that the flow stress decreases by increasing temperature and decreasing strain rate. In the initial process of deformation, dislocation multiplication causes the work hardening and then flow stress increases to a peak point which indicates the occurrence of dynamic recrystallization (DRX). The flow, curves without an obvious peak point with a steady state regime, which generally illustrates the dynamic recovery (DRV) [43, 44]. As is observed in Fig. 1(a), the flow stress decreases by increasing the strain rate. This anomalous behavior indicates the dynamic strain aging (DSA) phenomenon [45]. Due to DSA, the negative strain rate sensitivity has been seen at the temperature of 973 K. The (i) negative strain rate sensitivity and (ii) serrated flow curve are considered as the main clues for the occurrence of dynamic strain ageing. In some cases, the serration may be too fine to be observed at specified thermomechanical conditions [46, 47].

3.2. Johnson-Cook model

The Johnson-Cook equation shows the impact of deformation temperature (T), strain rate ($\dot{\epsilon}$) and strain (ϵ) on flow stress (σ) as follows:

$$\sigma = (A + B\epsilon^n)(1 + C\ln\dot{\epsilon}^*) (1 - T^{*m}) \quad (1)$$

where A is the yield stress at reference strain rate and

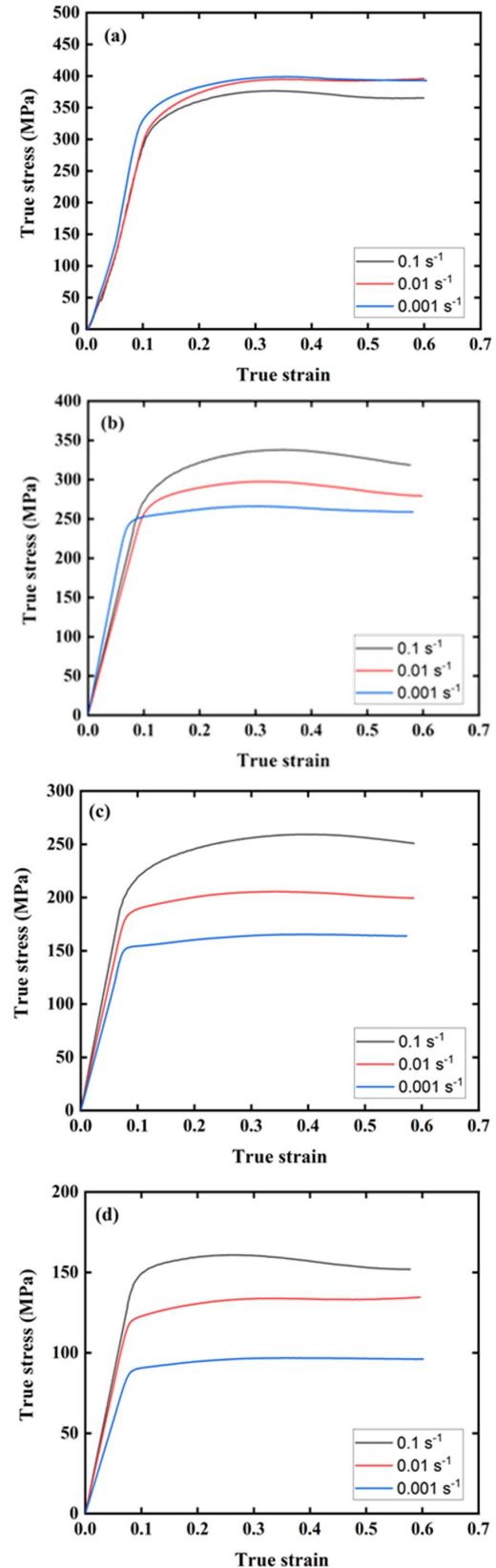


Fig. 1. The high temperature flow behavior of SLMed 316L stainless steel at the temperature of (a) 973 K, (b) 1073 K, (c) 1173 K, and (d) 1273 K.

reference temperature ($A=136.173$ MPa), B is strain hardening coefficient, n is strain hardening exponent, C is strain rate hardening coefficient, and m is thermal softening exponent. Additionally, $\dot{\epsilon}^* = \dot{\epsilon}/\dot{\epsilon}_0$ is dimensionless strain rate and $\dot{\epsilon}_0$ is the reference strain rate while $T^* = (T - T_r)/(T_m - T_r)$ represents homologous temperature with T_r being the reference temperature, and T_m the melting temperature (1659 K for the experimental alloy). In this investigation, 0.001 s^{-1} (lowest strain rate) and 973 K (lowest temperature) are taken as reference strain rates ($\dot{\epsilon}_0$) and reference temperatures (T_r), respectively. At the reference temperature and strain rate, Eq. (1) can be simplified as:

$$\sigma = A + B\epsilon^n \quad (2)$$

Taking the natural logarithm on both sides of Eq. (2) gives:

$$\ln(\sigma - A) = \ln B + n \ln \epsilon \quad (3)$$

In order to calculate the constants n and B , the relationship between $\ln(\sigma - A)$ and $\ln \epsilon$ is plotted in Fig. 2. Constants n and B can be gained from the slope and intercept of the fitting line in the $\ln(\sigma - A)$ - $\ln \epsilon$ plot. Accordingly, n and B are calculated to be 0.144 and 296.397 MPa, respectively. When the temperature is 973 K, Eq. (1) can be written as follows:

$$\frac{\sigma}{A + B\epsilon^n} = 1 + C \ln \dot{\epsilon}^* \quad (4)$$

The relationship between $\sigma/(A + B\epsilon^n)$ and $\ln \dot{\epsilon}^*$ for series of strains (0.1-0.5) is shown in Fig. 3. The value of C is obtained from the slope of the fitting line in Fig. 3, which is equal to -0.015. When the strain rate is 0.001 s^{-1} , Eq. (1) can be expressed as:

$$\frac{\sigma}{A + B\epsilon^n} = 1 - T^{*m} \quad (5)$$

Taking the natural logarithm on both sides of Eq. (5) results in:

$$\ln \left[1 - \frac{\sigma}{A + B\epsilon^n} \right] = m \ln T^* \quad (6)$$

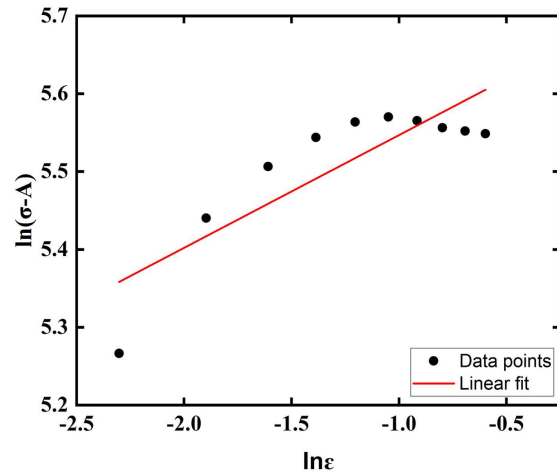


Fig. 2. The relationship between $\ln(\sigma - A)$ and $\ln \epsilon$ at the reference temperature and reference strain rate.

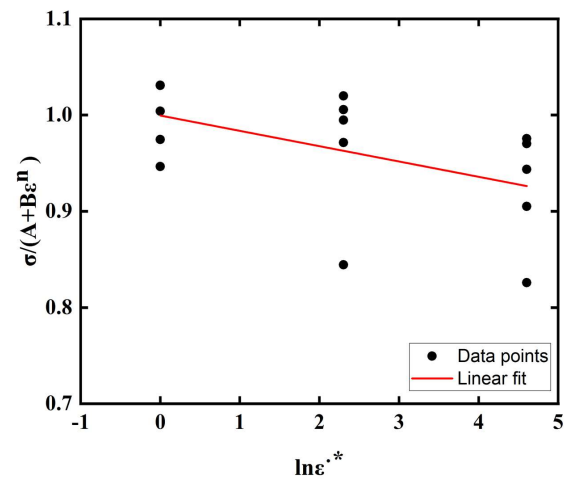


Fig. 3. The relationship between $\sigma/(A + B\epsilon^n)$ and $\ln \dot{\epsilon}^*$ at the reference temperature (973 K).

By substituting the values of flow stresses at different strains under deformation temperatures (973, 1073, 1173, and 1273 K) into Eq. (6), the relationship between $\ln[1 - \sigma/(A + B\epsilon^n)]$ and $\ln T^*$ is plotted in Fig. 4. The material constant m is calculated as 0.806 by linear fitting method. After determining the constants of the Johnson-Cook model, Eq. (1) can be summarized as:

$$\sigma = (136.173 + 296.397\epsilon^{0.1448}) (1 + (-0.0159)\ln \dot{\epsilon}^*) (1 - T^{*0.806}) \quad (7)$$

The comparisons between the experimental and predicted flow stress values by the Johnson-Cook model are shown in Fig. 5. As observed, this model is incapable of accurately predicting the flow stress over the whole

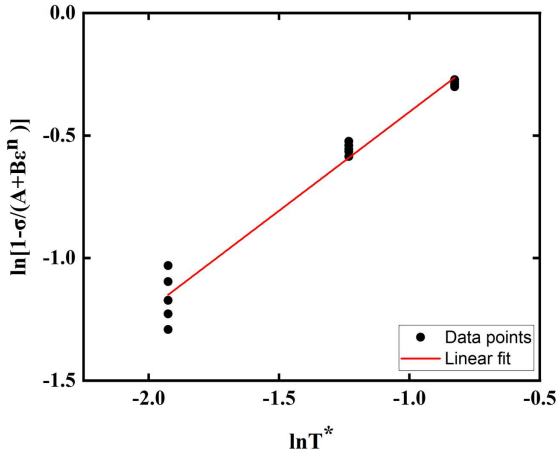


Fig. 4. The relationship between $\ln[1 - \sigma / (A + B\epsilon^n)]$ and $\ln T^*$ at the reference strain rate (0.001 s^{-1}).

temperatures and strain rates. Prediction can only be acceptable in reference temperature and strain rates. Furthermore, the Johnson-Cook model cannot predict the flow softening behavior of materials.

3.3. Arrhenius-type model

The influence of temperature (T) and strain rate ($\dot{\epsilon}$) on flow stress (σ) can be represented by the Arrhenius-type model as follows:

$$\dot{\epsilon} = A_1 \sigma^{n_1} \exp\left(-\frac{Q}{RT}\right) \quad (\alpha\sigma < 0.8) \quad (8)$$

$$\dot{\epsilon} = A_2 \exp(\beta\sigma) \exp\left(-\frac{Q}{RT}\right) \quad (\alpha\sigma > 1.2) \quad (9)$$

$$\dot{\epsilon} = A[\sinh(\alpha\sigma)]^n \exp\left(-\frac{Q}{RT}\right) \quad (\text{for all } \sigma) \quad (10)$$

where Q is the activation energy (kJ/mol), R is the universal gas constant (8.314 J/mol.K) and A_1 , A_2 , A , n_1 , n , β , and α are the material constants.

In addition, the Zener-Hollomon parameter (Z) can be used to describe the relationship between temperature, strain rate and deformation behaviors as shown in Eq. (11).

$$Z = \dot{\epsilon} \exp\left(\frac{Q}{RT}\right) \quad (11)$$

In order to determine the material constants, the strain of 0.2 and corresponding flow stress values were chosen

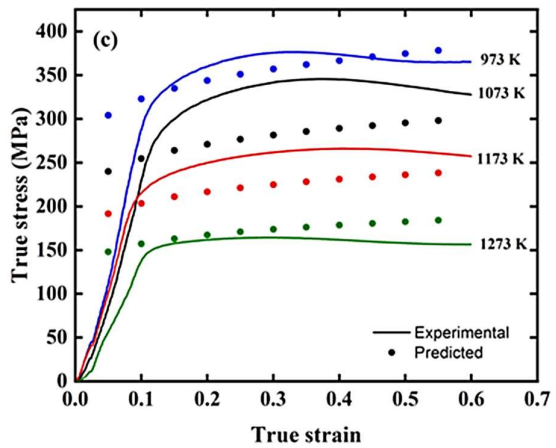
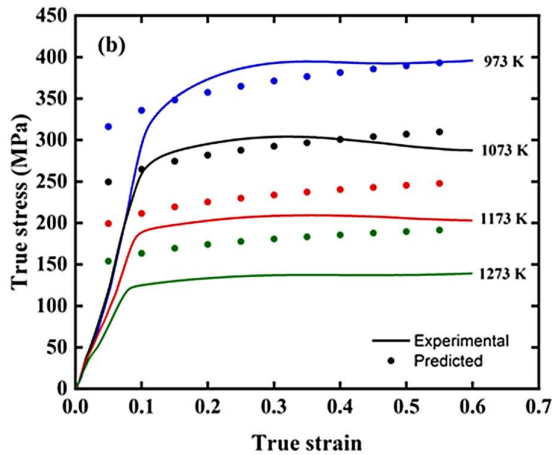
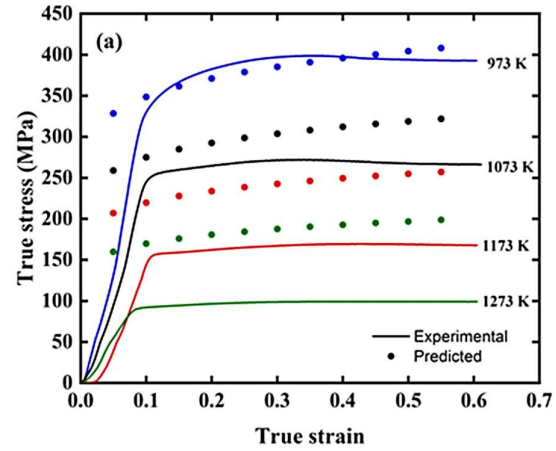


Fig. 5. The comparisons between the experimental and predicted flow stress values by the Johnson-Cook model under the strain rate of (a) 0.001 s^{-1} , (b) 0.01 s^{-1} , and (c) 0.1 s^{-1} .

at different strain rates and deformation temperatures. Taking the natural logarithm on both sides of Eq. (8) and Eq. (9), leads to:

$$\ln \dot{\epsilon} = \ln A_1 + n_1 \ln \sigma - \left(\frac{Q}{RT}\right) \quad (12)$$

$$\ln \dot{\epsilon} = \ln A_2 + \beta \sigma - \left(\frac{Q}{RT} \right) \quad (13)$$

The values of n_1 and β can be obtained from the mean slopes of fitting lines in the $\ln \dot{\epsilon}$ - $\ln \sigma$ and $\ln \dot{\epsilon}$ - σ plots, respectively in Fig. 6. As is shown in Fig. 6, the negative slope of 973 K indicates the dynamic strain aging (DSA) phenomenon. Therefore, in order to avoid errors in the slope averaging process, the values of 973 K were omitted. Material constants n_1 and β are calculated to be 13.968 and 0.067 MPa^{-1} , respectively. Moreover, α ($\alpha = \beta/n_1$) is determined as 0.0048 MPa^{-1} .

For all the stress levels, taking the natural logarithm on both sides of Eq. (10), Eq. (14) can be expressed as:

$$\ln \dot{\epsilon} = \ln A + n \ln[\sinh(\alpha \sigma)] - \left(\frac{Q}{RT} \right) \quad (14)$$

The relationship between $\ln \dot{\epsilon}$ and $\ln[\sinh(\alpha \sigma)]$

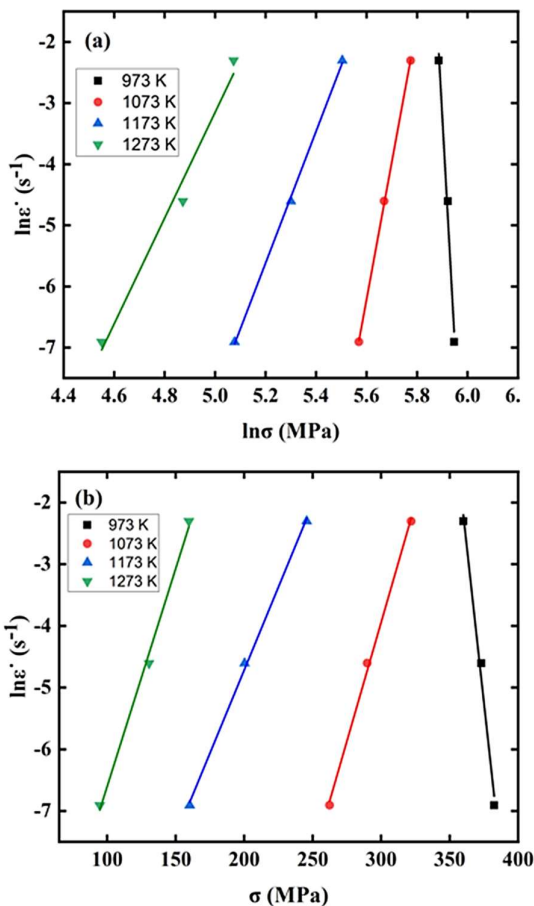


Fig. 6. The relationship between (a) $\ln \dot{\epsilon}$ and $\ln \sigma$, (b) $\ln \dot{\epsilon}$ and σ .

under deformation temperatures of 1073, 1173, and 1273 K is plotted in Fig. 7. The value of n is determined to be 10.095 from the mean slopes of fitting lines in Fig. 7. By rearranging Eq. (14), the activation energy (Q) can be obtained from the following equation:

$$Q = nR \frac{\partial \ln[\sinh(\alpha \sigma)]}{\partial \left(\frac{1}{T} \right)} \quad (15)$$

For this purpose, the relationship between $\ln[\sinh(\alpha \sigma)]$ and $1/T$ is plotted in Fig. 8. The Q value is found to be 619.564 kJ/mol. Comparatively, the activation energy for conventionally fabricated 316LN and 316L under the same thermomechanical condition were extracted from the previous works, which were found to be 487-549 kJ/mol [48] and 100-200 kJ/mol [49],

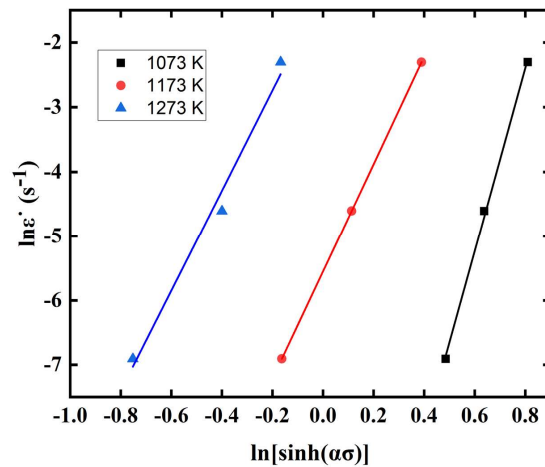


Fig. 7. The relationship between $\ln \dot{\epsilon}$ and $\ln[\sinh(\alpha \sigma)]$.

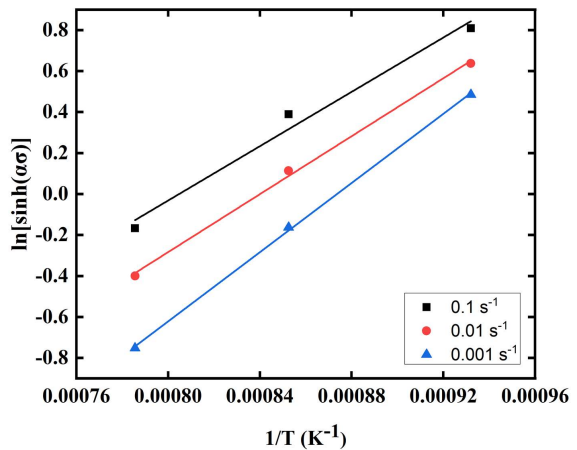


Fig. 8. The relationship between $\ln[\sinh(\alpha \sigma)]$ and $1/T$.

respectively. Consequently, SLMed 316L stainless steel possesses higher activation energy than those manufactured through conventional methods. According to Eq. (10) and Eq. (11), the following equation can be expressed as:

$$Z = A[\sinh(\alpha\sigma)]^n \quad (16)$$

Taking the natural logarithm on both sides of Eq. (16) gives:

$$\ln Z = \ln A + n \ln[\sinh(\alpha\sigma)] \quad (17)$$

$\ln A$ can be gained from the intercept of fitting lines in the $\ln Z$ - $\ln[\sinh(\alpha\sigma)]$ plot in Fig. 9. In the next step, the material constant A is calculated as 1.874×10^{25} . The n -value can be more precisely recalculated from the of fitting line's slope in Fig. 9, where the temperature, strain rate and stress has been correlated through introducing the Z -parameter. Consequently, the n -value was determined to be 9.850.

After determining the material constants, the Arrhenius-type equation and Zener-Hollomon parameter can be expressed as follows:

$$\dot{\epsilon} = 1.874 \times 10^{25} [\sinh(0.00481 \times \sigma)]^{9.850} \exp\left(-\frac{619546}{RT}\right) \quad (18)$$

$$Z = \dot{\epsilon} \exp\left(\frac{619546}{RT}\right)$$

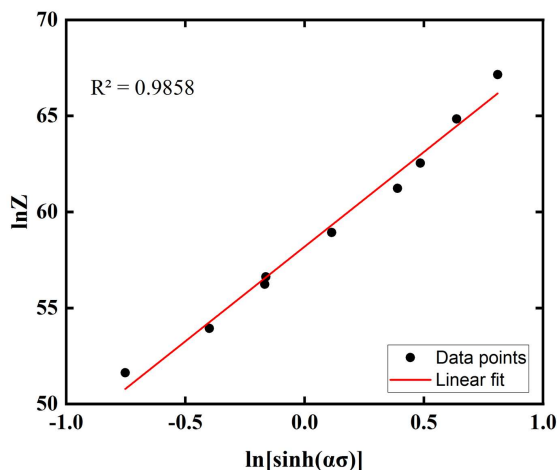


Fig. 9. The relationship between $\ln Z$ and $\ln[\sinh(\alpha\sigma)]$.

The comparisons between the experimental and predicted data by the Arrhenius-type model for all experimental temperatures and without temperature of 973 K are shown in Fig. 10, respectively. As is seen, by removing the temperature of 973 K, the accuracy of the Arrhenius-type model increases.

3.4. Artificial neural network model

The ANN model is an artificial intelligence approach which is capable of mimicing complicate relationships by using neurons as processing units [50]. In this study, a multilayer perceptron (MLP) with feed-forward back propagation learning algorithm has been employed to predict the high temperature flow behavior of SLMed 316L stainless steel. The MLP consists of an input layer, one or more hidden layers and an output layer which are connected with neurons. The input layer variables are true strain (ϵ), strain rate ($\dot{\epsilon}$) and deformation temperature (T). The flow stress (σ) is considered as the

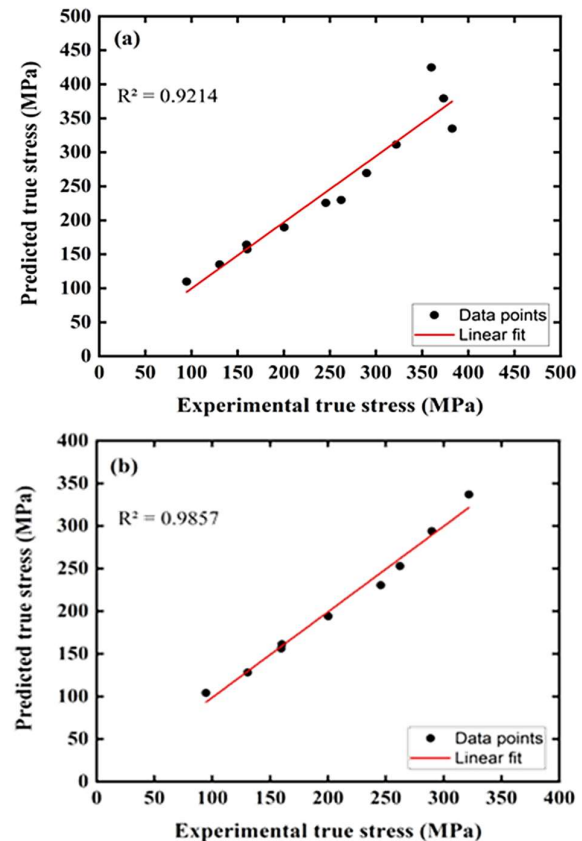


Fig. 10. Comparisons between the experimental and predicted flow stresses by Arrhenius-type model (a) all experimental temperatures, (b) without temperature of 973 K.

output data. The number of hidden layers and the neurons inside them can be the variable. In this respect, the ANN model has been trained for different numbers of hidden layers and neurons. As is shown in Fig. 11, the network with one hidden layer and 20 neurons has the optimal performance and the least mean square error (MSE). The structure of back propagation of the ANN model is depicted in Fig. 12.

Before training, the network, input and output values were normalized between 0 and 1 by the following equation:

$$X_N = 0.1 + 0.8 \left(\frac{X - X_{\min}}{X_{\max} - X_{\min}} \right) \quad (19)$$

where X_N is the normalized data, X is the original data, X_{\min} is the minimum value of X and X_{\max} is the maximum value of X . The Levenberg-Marquardt algorithm is utilized to train the network. In the current ANN model, 420 experimental data sets have been selected from the true stress-true strain curves in the strain

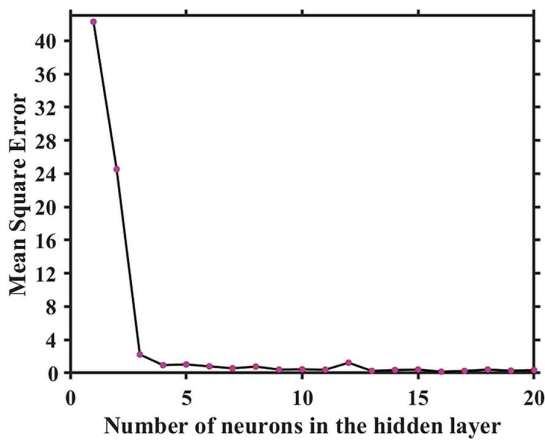


Fig. 11. The effect of various numbers of neurons on the performance of ANN model.

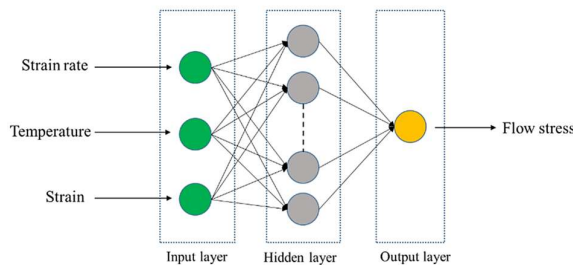


Fig. 12. The structure of back propagation ANN architecture.

range of 0.01-0.6 with an interval of 0.02. 315 data sets have been utilized to train the network, and the rest of the data sets (105 data) have been employed for testing the model.

Fig. 13 shows the comparisons between the experimental and predicted values by the ANN model. As is observed, the predicted data can well track both the hardening and softening behavior of material during hot deformation.

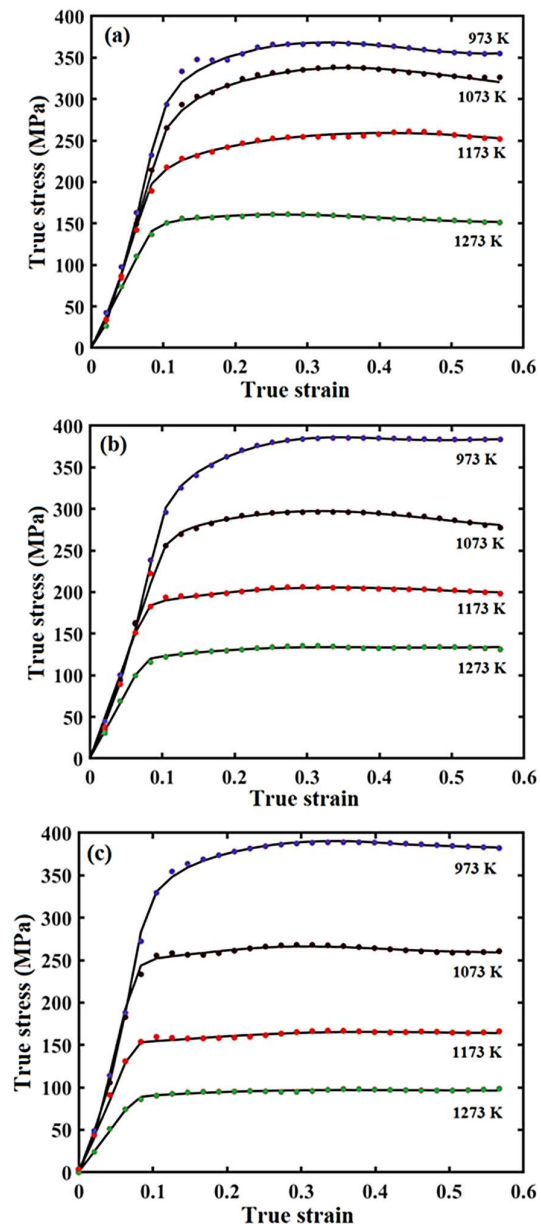


Fig. 13. The comparisons between the experimental and predicted flow stress values by the ANN model under the strain rate of (a) 0.1 s^{-1} , (b) 0.01 s^{-1} , and (c) 0.001 s^{-1} .

3.5. Comparison between the employed models

To evaluate the prediction accuracy of the Johnson-Cook model, Arrhenius-type equation and ANN model, standard statistical parameters such as correlation coefficient (R), root mean square error (RMSE), and average absolute relative error (AARE) were employed as follows:

$$R = \frac{\sum_{i=1}^N (E_i - \bar{E})(P_i - \bar{P})}{\sqrt{\sum_{i=1}^N (E_i - \bar{E})^2 \sum_{i=1}^N (P_i - \bar{P})^2}} \quad (20)$$

$$RMSE = \sqrt{\frac{1}{N} \sum_{i=1}^N (E_i - P_i)^2} \quad (21)$$

$$AARE(\%) = \frac{1}{N} \sum_{i=1}^N \left| \frac{E_i - P_i}{E_i} \right| \times 100 \quad (22)$$

where E_i is the experimental data, P_i is the predicted value, \bar{E} and \bar{P} are the mean values of E_i and P_i , respectively. N is the total number of data that have been employed in the investigation. The correlation coefficient (R) shows the strength of the linear relationship between the experimental and predicted values. In addition, RMSE and AARE have been utilized to verify the predictability of employed models as unbiased statistical parameters [51]. The corresponding values of R, RMSE, and AARE have been listed in Table 3. The results indicate that the Arrhenius-type equation has performed better than the Johnson-Cook model. Additionally, with the removal of 973 K data, the accuracy of the Arrhenius-type model has increased. Among these models, the ANN model has the best R, RMSE, and AARE.

Table 3. The values of R, RMSE and AARE for the constitutive models and ANN model

Model	R	RMSE	AARE (%)
Johnson-Cook	0.964	73.171	47.988
Arrhenius-type	0.960	27.236	7.706
Arrhenius-type (without 973 K)	0.992	8.838	3.734
ANN	0.9997	1.51	2.82

4. Conclusion

The hot flow behavior of 316L stainless steel manufactured by the selective laser melting (SLM) process, was investigated through the phenomenological constitutive models and the ANN model at the temperatures of 973, 1073, 1173, and 1273 K under the strain rates of 0.001, 0.01, and 0.1 s⁻¹. The Johnson-Cook model showed a poor prediction only acceptable in reference conditions. Although the Arrhenius-type model performed better than the Johnson-Cook model, it could not predict the dynamic strain aging (DSA) effect at the temperature of 973 K. In addition, the significant effect of imposed strain was not considered in the Arrhenius-type equation. The activation energy (Q) was calculated to be 619.564 kJ/mol. The ANN model with 20 neurons in one hidden layer accurately predicted the flow stress. Interestingly, the ANN model predicts both the hardening and softening regions over the whole temperatures and strain rates. The predictability of employed models was evaluated through the standard statistical parameters. The results showed that the ANN model can predict hot flow behavior better than constitutive models. R, RMSE, and AARE for the ANN model were found to be 0.9997, 1.51, and 2.82%, respectively.

Funding

This research received no specific grant from any funding agency in the public, commercial, or not-for-profit sectors.

Conflict of Interests

The authors declare that they have no known competing financial interests or personal relationships that could have appeared to influence the work reported in this paper.

5. References

- [1] Y. Yin, Q. Tan, M. Bermingham, N. Mo, J. Zhang, M.X. Zhang, Laser additive manufacturing of steels, *International Materials Reviews*, 67(5) (2022) 487-573.

- [2] A. Habibiyan, A. Hanzaki, H.R. Abedi, An investigation into microstructure and high-temperature mechanical properties of selective laser-melted 316L stainless steel toward the development of hybrid Ampliforge process, *The International Journal of Advanced Manufacturing Technology*, 110(1) (2020) 383-394.
- [3] W.E. Frazier, Metal additive manufacturing: a review, *Journal of Materials Engineering and Performance*, 23(6) (2014) 1917-1928.
- [4] S.I. Shakil, N.R. Smith, S.P. Yoder, B.E. Ross, D.J. Alvarado, A. Hadadzadeh, M. Haghshenas, Post fabrication thermomechanical processing of additive manufactured metals: a review, *Journal of Manufacturing Processes*, 73 (2022) 757-790.
- [5] K. Lin, D. Gu, L. Xi, L. Yuan, S. Niu, P. Lv, Q. Ge, Selective laser melting processing of 316L stainless steel: effect of microstructural differences along building direction on corrosion behavior, *The International Journal of Advanced Manufacturing Technology*, 104(5) (2019) 2669-2679.
- [6] A.B. Kale, B.K. Kim, D.I. Kim, E.G. Castle, M. Reece, S.H. Choi, An investigation of the corrosion behavior of 316L stainless steel fabricated by SLM and SPS techniques, *Materials Characterization*, 163 (2020) 110204.
- [7] H. Attar, M. Calin, L.C. Zhang, S. Scudino, J. Eckert, Manufacture by selective laser melting and mechanical behavior of commercially pure titanium, *Materials Science and Engineering: A*, 593 (2014) 170-177.
- [8] J. Suryawanshi, K.G. Prashanth, U. Ramamurty, Mechanical behavior of selective laser melted 316L stainless steel, *Materials Science and Engineering: A*, 696 (2017) 113-121.
- [9] S. Papula, M. Song, A. Pateras, X.B. Chen, M. Brandt, M. Easton, Y. Yagodzinsky, I. Virkkunen, H. Hänninen, Selective laser melting of duplex stainless steel 2205: effect of post-processing heat treatment on microstructure, mechanical properties, and corrosion resistance, *Materials*, 12(15) (2019) 2468.
- [10] W.M. Tucho, V.H. Lysne, H. Austbø, A. Sjolyst-Kverneland, V. Hansen, Investigation of effects of process parameters on microstructure and hardness of SLM manufactured SS316L, *Journal of Alloys and Compounds*, 740 (2018) 910-925.
- [11] A.B. Kale, J. Singh, B.K. Kim, D.I. Kim, S.H. Choi, Effect of initial microstructure on the deformation heterogeneities of 316L stainless steels fabricated by selective laser melting processing, *Journal of Materials Research and Technology*, 9(4) (2020) 8867-8883.
- [12] H. Mirzadeh, J.M. Cabrera, A. Najafzadeh, Modeling and prediction of hot deformation flow curves, *Metallurgical and Materials Transactions A*, 43(1) (2012) 108-123.
- [13] M.O. Bodunrin, Flow stress prediction using hyperbolic-sine Arrhenius constants optimised by simple generalised reduced gradient refinement, *Journal of Materials Research and Technology*, 9(2) (2020) 2376-2386.
- [14] E. Farabi, A. Zarei-Hanzaki, H.R. Abedi, High temperature formability prediction of dual phase brass using phenomenological and physical constitutive models, *Journal of Materials Engineering and Performance*, 24(1) (2015) 209-220.
- [15] M.K. Razali, M. Irani, M. Joun, General modeling of flow stress curves of alloys at elevated temperatures using bi-linearly interpolated or closed-form functions for material parameters, *Journal of Materials Research and Technology*, 8(3) (2019) 2710-2720.
- [16] M.S. Joun, M.K. Razali, S.H. Chung, M. Irani, A direct method of calculating flow-related dynamic recrystallization parameters for generality and accuracy in predicting microstructural evolution, *Journal of Materials Research and Technology*, 18 (2022) 3894-3907.
- [17] M.S. Joun, M.K. Razali, J.D. Yoo, M.C. Kim, J.M. Choi, Novel extended Cm models of flow stress for accurate mechanical and metallurgical calculations and comparison with traditional flow models, *Journal of Magnesium and Alloys*, (2021).
- [18] M.S. Joun, M.K. Razali, C.W. Jee, J.B. Byun, M.C. Kim, K.M. Kim, A review of flow characterization of metallic materials in the cold forming temperature range and its major issues, *Materials*, 15(8) (2022) 2751.
- [19] G.R. Johnson, A constitutive model and data for materials subjected to large strains, high strain rates, and high temperatures, *Seventh International Symposium on Ballistics: Proceedings*, (1983) 541-547.
- [20] A. Abbasi-Bani, A. Zarei-Hanzaki, M.H. Pishbin, N. Haghdad, A comparative study on the capability of Johnson-Cook and Arrhenius-type constitutive equations to describe the flow behavior of Mg-6Al-1Zn alloy, *Mechanics of Materials*, 71 (2014) 52-61.
- [21] X. Chen, Q. Liao, Y. Niu, W. Jia, Q. Le, C. Cheng, F. Yu, J. Cui, A constitutive relation of AZ80 magnesium alloy during hot deformation based on Arrhenius and Johnson-Cook model, *Journal of Materials Research and Technology*, 8(2) (2019) 1859-1869.
- [22] Z. Xie, Y. Guan, J. Lin, J. Zhai, L. Zhu, Constitutive model of 6063 aluminum alloy under the ultrasonic vibration upsetting based on Johnson-Cook model, *Ultrasonics*, 96 (2019) 1-9.
- [23] L. Niu, M. Cao, Z. Liang, B. Han, Q. Zhang, A modified Johnson-Cook model considering strain softening of

- A356 alloy, *Materials Science and Engineering: A*, 789 (2020) 139612.
- [24] M.E. Korkmaz, Verification of Johnson-Cook parameters of ferritic stainless steel by drilling process: experimental and finite element simulations, *Journal of Materials Research and Technology*, 9(3) (2020) 6322-6330.
- [25] Z. Akbari, H. Mirzadeh, J.M. Cabrera, A simple constitutive model for predicting flow stress of medium carbon microalloyed steel during hot deformation, *Materials & Design*, 77 (2015) 126-131.
- [26] J. He, F. Chen, B. Wang, L.B. Zhu, A modified Johnson-Cook model for 10%Cr steel at elevated temperatures and a wide range of strain rates, *Materials Science and Engineering: A*, 715 (2018) 1-9.
- [27] Y. Prawoto, M. Fanone, S. Shahedi, M.S. Ismail, W.B. Wan Nik, Computational approach using Johnson-Cook model on dual phase steel, *Computational Materials Science*, 54 (2012) 48-55.
- [28] S. Yadav, S. Singhal, Y. Jasra, R.K. Saxena, Determination of Johnson-Cook material model for weldment of mild steel, *Materials Today: Proceedings*, 28 (2020) 1801-1808.
- [29] N. Raut, S. Shinde, V. Yakkundi, Determination of Johnson Cook parameters for Ti-6Al-4V Grade 5 experimentally by using three different methods, *Materials Today: Proceedings*, 44 (2021) 1653-1658.
- [30] S. Deb, A. Muraleedharan, R.J. Immanuel, S.K. Panigrahi, G. Racineux, S. Marya, Establishing flow stress behaviour of Ti-6Al-4V alloy and development of constitutive models using Johnson-Cook method and artificial neural network for quasi-static and dynamic loading, *Theoretical and Applied Fracture Mechanics*, 119 (2022) 103338.
- [31] C.M. Sellars, W.J. McTegart, On the mechanism of hot deformation, *Acta Metallurgica*, 14(9) (1966) 1136-1138.
- [32] H.R. Rezaei Ashtiani, P. Shahsavari, A comparative study on the phenomenological and artificial neural network models to predict hot deformation behavior of AlCuMgPb alloy, *Journal of Alloys and Compounds*, 687 (2016) 263-273.
- [33] Y.C. Lin, J. Zhang, J. Zhong, Application of neural networks to predict the elevated temperature flow behavior of a low alloy steel, *Computational Materials Science*, 43(4) (2008) 752-758.
- [34] S.A. Sani, G.R. Ebrahimi, H. Vafaenezhad, A.R. Kiani-Rashid, Modeling of hot deformation behavior and prediction of flow stress in a magnesium alloy using constitutive equation and artificial neural network (ANN) model, *Journal of Magnesium and Alloys*, 6(2) (2018) 134-144.
- [35] G.Z. Quan, C.T. Yu, Y.Y. Liu, Y.F. Xia, A comparative study on improved arrhenius-type and artificial neural network models to predict high-temperature flow behaviors in 20MnNiMo Alloy, *The Scientific World Journal*, 2014 (2014) 108492.
- [36] N. Haghdadi, A. Zarei-Hanzaki, A.R. Khalesian, H.R. Abedi, Artificial neural network modeling to predict the hot deformation behavior of an A356 aluminum alloy, *Materials & Design*, 49 (2013) 386-391.
- [37] Y. Sun, W.D. Zeng, Y.Q. Zhao, X.M. Zhang, X. Ma, Y.F. Han, Constructing processing map of Ti40 alloy using artificial neural network, *Transactions of Nonferrous Metals Society of China*, 21(1) (2011) 159-165.
- [38] I.Y. Moon, H.W. Jeong, H.W. Lee, S.J. Kim, Y.S. Oh, J. Jung, S.H. Kang, Predicting high temperature flow stress of nickel alloy A230 based on an artificial neural network, *Metals*, 12(2) (2022) 223.
- [39] M.T. Anaraki, M. Sanjari, A. Akbarzadeh, Modeling of high temperature rheological behavior of AZ61 Mg-alloy using inverse method and ANN, *Materials & Design*, 29(9) (2008) 1701-1706.
- [40] P. Wan, H. Zou, K. Wang, Z. Zhao, Research on hot deformation behavior of Zr-4 alloy based on PSO-BP artificial neural network, *Journal of Alloys and Compounds*, 826 (2020) 154047.
- [41] H. Yang, H. Bu, M. Li, X. Lu, Prediction of flow stress of annealed 7075 Al alloy in hot deformation using strain-compensated arrhenius and neural network models, *Materials*, 14(20) (2021) 5986.
- [42] ASTM E209-18, Standard practice for compression tests of metallic materials at elevated temperatures with conventional or rapid heating rates and strain rates, ASTM International, 2018.
- [43] D.X. Wen, Y.C. Lin, H.B. Li, X.M. Chen, J. Deng, L.T. Li, Hot deformation behavior and processing map of a typical Ni-based superalloy, *Materials Science and Engineering: A*, 591 (2014) 183-192.
- [44] J. Zhang, H. Di, K. Mao, X. Wang, Z. Han, T. Ma, Processing maps for hot deformation of a high-Mn TWIP steel: A comparative study of various criteria based on dynamic materials model, *Materials Science and Engineering: A*, 587 (2013) 110-122.
- [45] A. Moris Devotta, P.V. Sivaprasad, T. Beno, M. Eynian, K. Hjertig, M. Magnevall, M. Lundblad, A modified Johnson-Cook model for ferritic-pearlitic atel in dynamic strain aging regime, *Metals*, 9(5) (2019) 528.
- [46] R. Khani, A. Zarei-Hanzaki, A. Moshiri, H.R. Abedi, S.S. Sohn, Dynamic strain aging and twin formation during warm deformation of a novel medium-entropy lightweight steel, *Journal of Materials Research and Technology*, 17 (2022) 1628-1641.

- [47] H.R. Abedi, A. Zarei Hanzaki, N. Nemati, D.E. Kim, Trading off between dynamic strain aging and substructure evolution in κ -carbide-free lightweight steel at room temperature, *Scripta Materialia*, 157 (2018) 110-114.
- [48] M.W. Guo, Z.H. Wang, Z.A. Zhou, S.H. Sun, W.T. Fu, Effect of nitrogen content on hot deformation behavior and grain growth in nuclear grade 316LN stainless steel, *Advances in Materials Science and Engineering*, 2015 (2015) 427945.
- [49] D. Samantaray, S. Mandal, V. Kumar, S.K. Albert, A.K. Bhaduri, T. Jayakumar, Optimization of processing parameters based on high temperature flow behavior and microstructural evolution of a nitrogen enhanced 316L(N) stainless steel, *Materials Science and Engineering: A*, 552 (2012) 236-244.
- [50] G. Ji, F. Li, Q. Li, H. Li, Z. Li, A comparative study on Arrhenius-type constitutive model and artificial neural network model to predict high-temperature deformation behaviour in Aermet100 steel, *Materials Science and Engineering: A*, 528(13-14) (2011) 4774-4782.
- [51] O. Sabokpa, A. Zarei-Hanzaki, H.R. Abedi, N. Haghdadi, Artificial neural network modeling to predict the high temperature flow behavior of an AZ81 magnesium alloy, *Materials & Design*, 39 (2012) 390-396.